MNRAS **000**, 1–10 (2018) Preprint 10 March 2024 Compiled using MNRAS LATEX style file v3.0

A 6.7 GHz methanol maser survey of the central molecular zone

Matthew Rickert[1,2], F. Yusef-Zadeh[1], and J. Ott[2]
[1]*CIERA and Department of Physics and Astronomy, Northwestern University, 2145 Sheridan Rd., Evanston, IL 60208-3112, USA*
[2]*National Radio Astronomy Observatory, 1003 Lopezville Rd, Socorro, NM 87801*

Accepted XXX. Received 10 March 2024; in original form 9 August 2018

arXiv:1812.05730v2 [astro-ph.GA] 4 Jan 2019

ABSTRACT

The Central Molecular Zone (CMZ) spans the inner ~450 pc (~3°) of our Galaxy. This region is defined by its enhanced molecular emission and contains 5% of the entire Galaxy's molecular gas mass. However, the number of detected star forming sites towards the CMZ may be low for the amount of molecular gas that is present, and improved surveys of star formation indicators can help clarify this. With the Karl G Jansky Very Large Array (VLA), we conducted a blind survey of 6.7 GHz methanol (CH_3OH) masers spanning the inner 3°× 40′ (450 pc × 100 pc) of the Galaxy. We detected 43 CH_3OH masers towards 28 locations, ~16 of which are new detections. The velocities of most of these masers are consistent with being located within the CMZ. A majority of the detected CH_3OH masers are distributed towards positive Galactic longitudes, similar to 2/3 of the molecular gas mass distributed at positive Galactic longitudes. The 6.7 GHz CH_3OH maser is an excellent indicator of high mass ($> 8M_\odot$) star formation, with new detections indicating sites of massive star formation in the CMZ.

Key words: Galaxy: center—Galaxy: nucleus—star formation — catalogs — surveys

1 INTRODUCTION

The Central Molecular Zone (CMZ) occupies the inner ~ 450 pc (~ 3°) of the Galaxy. This region is defined by enhanced molecular gas emission. While being less than 1% of the Galaxy's volume, it is estimated to contain 5% of the Galaxy's molecular gas mass (Xu et al. 2015; Dahmen et al. 1998). The ISM in the CMZ is unique in its physical properties, containing a higher molecular gas density (Ao et al. 2013), higher temperature (Ao et al. 2013; Oka et al. 2005; Martin et al. 2004; Morris & Serabyn 1996), and increased turbulent velocity (Ao et al. 2013; Lis & Menten 1998; Martín-Pintado et al. 1997; Morris & Serabyn 1996; Bally et al. 1987) than elsewhere in the Galaxy.

How star formation progresses in the unique environment of the CMZ is a current research topic. While the CMZ contains a relatively high star formation rate (SFR) of ~ $0.1M_\odot\ yr^{-1}$, the large molecular gas mass calls into question the efficiency of star formation in this environment (Barnes et al. 2017; Longmore et al. 2013). Longmore et al. (2013) show that the fraction of the number of star formation indicators per fraction of dense gas is lower in the CMZ than in the Galactic disk, implying that the star formation is suppressed in the CMZ. Yusef-Zadeh et al. (2009) instead have shown that the CMZ falls along the Kennicut-Schmidt relation, indicating that the CMZ star formation is neither suppressed nor enhanced. While one of the ways to address this issue is to better constrain the molecular gas mass in the CMZ, we have instead chosen to address this issue by obtaining improved counts of the number of star forming sites in the CMZ.

Due to 30 magnitudes of visual extinction in the direction of the CMZ, masers are useful probes of star formation in the CMZ. We conducted the first blind interferometric survey of 6.7 GHz methanol (CH_3OH) masers towards the CMZ using the Jansky Very Large Array (VLA). This maser is a strong indicator of high mass ($> 8M_\odot$) star formation (Minier et al. 2003; van Dishoeck & Blake 1998). Unlike other CH_3OH masers (i.e 36, 44, 96 GHz), the 6.7 GHz CH_3OH maser is radiatively pumped by photons from dust heated by high mass stars (Menten 1991). The 6.7 GHz CH_3OH maser is solely associated with star formation (Breen et al. 2013), unlike other masers that are collisionally pumped (i.e. 36, 44, 96 GHz CH_3OH and 22 GHz H_2O) that can also be produced by shocks from clump-clump collisions.

Many of the previous surveys of young stellar objects (YSOs) cited in the works of Longmore et al. (2013) and Yusef-Zadeh et al. (2009) have utilized single dish telescopes and/or targeted surveys (i.e. Walsh et al. 2011; Chambers et al. 2014 and Caswell et al. 2011), which could cause the survey to miss detections. We instead use a blind interferometric survey with a large and uniform spatial coverage to obtain a sensitivity limited sample of masers.

2 OBSERVATIONS

We conducted a single survey of 6.7 GHz CH_3OH masers with the Karl G. Jansky Very Large Array (VLA[1]) on September 9,

[1] The VLA is operated by the National Radio Astronomy Observatory (NRAO), which is a facility of the National Science Foundation (NSF) operated under cooperative agreement by Associated Universities, Inc.

© 2018 The Authors

2015. The VLA was in its A-array configuration providing a spatial resolution of $0.83'' \times 0.29''$. Table 1 summarizes the observing setup, including the spectral resolution and velocity coverage.

The survey covers the inner $3^\circ \times 40'$ ($l \times b$) of the GC using 203 overlapping pointings with a standard Nyquist sampling to ensure near uniform sensitivity. Figure 5 shows these pointings over plotted on a 24 μmmap (Yusef-Zadeh et al. 2009). Each pointing was observed for 47 seconds and a total of $\sim$ 10 minutes was spent on calibrators. J1733-1304 was observed as a bandpass and gain calibrator and 3C286 was observed as a flux and bandpass calibrator. The initial desired noise level (based on the online VLA exposure calculator) of 0.01 Jy beam^{-1} was almost obtained for a majority of the resulting map, with the average RMS being 0.08 Jy beam^{-1} (Table 3 later shows the channel RMS near each of the detections).

2.1 Comparison to Previous Blind 6.7 GHz CH_3OH Maser Surveys of the CMZ

There have been two other blind surveys of 6.7 GHz CH_3OH masers that have covered the CMZ. Table 2 compares our survey (indicated as Rickert2018) to these two other blind surveys. All other 6.7 GHz CH_3OH maser surveys have either targeted specific sources or did not cover the CMZ. This is in part due to the lack of 6.7 GHz receivers on VLA and GBT that could observe this frequency in the past[2].

The most recent untargeted survey of 6.7 GHz CH_3OH masers covering the CMZ is the methanol multibeam (MMB) survey (Green et al. 2009). The MMB survey used the Parkes single dish telescope for their initial detections (although later followed up these detections with the Australia Telescope Compact Array (ATCA)). Our CH_3OH survey has a comparable sensitivity and higher initial resolution than the MMB survey (Caswell 1996).

Before the MMB survey, Chambers et al. (2009) also conducted a blind 6.7 GHz CH_3OH maser ATCA survey of the CMZ. Due to the configuration they were in, they had a poorer resolution ($2'' \times 4''$, 0.18 km s^{-1}) than the follow up ATCA observations used in the MMB survey. Although the spectral resolution of Chambers et al. (2009) is better than our VLA observations, their spatial resolution and sensitivity are both poorer than ours.

2.2 Data Reduction and Imaging

To reduce the large data set, the primary visibility file was split into mosaics of 7 fields in a Nyquist sampled mosaic pattern. This ensures that the central field contains the full survey sensitivity. Common Astronomy Software Applications (CASA, McMullin et al. 2007) was used as the primary reduction, calibration, imaging, and analysis package for this survey. The split visibility files were then continuum subtracted (using the CASA task *uvcontsub*) with line free channels near $\sim \pm 250$ km s^{-1} selected for fitting the continuum. Each field was imaged individually (with a cleaning threshold of 0.055 Jy and a maximum 200 iteration limit with a loop gain of 0.1) over just the central $\sim$ 230 km s^{-1} (as opposed to the full $\pm$ 390 km s^{-1}) and were then combined together using CASA's image.linearmosaic function into hexagonal patterns of 7 fields each. The resulting images were each 6750×6750 pixels (with a $0.1''$ pixel size and a $0.86'' \times 0.29''$ synthesized beam) with 570 channels (each 0.4 km s^{-1}, 8 kHz wide).

2.3 Maser Identification

Masers candidates were initially identified by creating peak maps of the central field of the 7 field mosaic. The CASA function *ia.findsource* was then used to identify all sources above 5 times the theoretical RMS (this resulted in initially a large number of false detections that were removed in a later step). Each maser candidate had a Gaussian fitted to its spectrum. This was done to prevent single channel detections and to distinguish between spectral peaks. If there were any sources near[3] each other in position and velocity then only the single maser candidate with the highest peak flux density was kept as a detection. The RMS was then measured by averaging the RMS from $\sim$ 5 regions (each $4''$ wide and located within $1'$ of the maser) within the channel of the spectral peak (this was to account for how the RMS may not be uniform throughout the survey). Finally, any sources whose fitted peak flux densities fell below 5 times this measured RMS were then removed, leaving a sensitivity limited catalog of sources that we were confident were masers. A similar method to this was used by Cotton & Yusef-Zadeh (2016), except that they used integrated maps, masked the channels before collapsing the image cube into an integrated map, and they did not fit Gaussians to their spectra.

3 RESULTS

We detected 43 CH_3OH maser candidates towards 28 distinct locations[4]. Table 3 gives the parameters of the Gaussian fit to each maser's spectrum. Columns 1-10 of Table 3 respectively give: the source ID[5], the Galactic coordinates, right ascension (RA), declination (Dec), peak flux density, RMS[6], central velocity, FWHM, integrated line intensity, and associated sources[7]. The Gaussian fit uncertainties are given for the flux density, velocity, FWHM, and integrated flux density.

Figure 2 shows the spectra for all the 43 CH_3OH masers. Each spectrum is labeled with the source ID and Galactic coordinates from Table 3. Within each spectrum, the identified spectral peaks are labeled with their corresponding velocities (from Table 3). Some of the spectra (such as those for sources 12, 20, 25, and 28) have apparent spectral peaks that do not have identified velocities. This is generally because: there is a brighter maser at the same velocity within 0.015°(and thus the unlabeled peak was deemed a potential artifact), the peak was below our detection limit, or a Gaussian could not be fitted to the spectrum (because it is only 1-2 channels wide). The channel width for these spectra[8] is 0.4 km s^{-1}.

[2] The current VLA C-band receivers (4–8 GHz) were not available on all the antennas before 2013 (van Moorsel 2013)

[3] Within 0.015° and the FWHM of the Gaussian fitted to each source's spectrum

[4] Compact sources $\sim 1''$ wide.

[5] The ID is in order of decreasing Galactic longitude.

[6] The RMS was measured in the channel of the peak maser emission from $\sim$ 5 regions (each $4''$ wide and located within $1'$ of the maser) and then averaged together.

[7] The associated sources are prominent features of the CMZ (i.e. Sgr A, Sgr B, etc.), references to sources from other catalogs (the footnotes indicate source type, catalog references, and the maximum distance between the CH_3OH maser and the catalog source), and indicators of new detections.

[8] Due to not having a narrower channel width, some of the bright and narrow masers display Gibbs ringing. Most modern interferometers record

3.1 Brightness Temperature

In order to verify the non-thermal nature of the detected CH_3OH maser candidates and support that they are masers, we determined the brightness temperature to distinguish them from thermal CH_3OH emission. The brightness temperature (T_b) is determined by:

$$T_b = \frac{c^2 S}{2k\nu^2\Omega}, \quad (1)$$

where c is the speed of light, k is the Boltzmann constant, ν is the frequency (6.66852 GHz), and Ω is the solid angle of the source. As these sources are spatially unresolved, we use a solid angle (Ω) equal to the synthesized beam ($0.86'' \times 0.29''$). S is the flux density in the peak channel integrated over the synthesized beam. This calculated brightness temperature is thus a lower limit on the actual brightness temperature, as it ignores the other channels that make up the spectrum and overestimates the angular size of the source. The second to last column of Table 3 lists these calculated minimum brightness temperatures (and the propagated error). The T_b values span $\sim 2 \times 10^3$ to $\sim 3 \times 10^6$ K. The molecular gas in the CMZ has temperatures <700 K. Given the high brightness temperatures and narrow line widths (<2.9 km s^{-1}, Table 3), the detected maser candidates are consistent with being masers.

4 DISCUSSION

The positive Galactic longitudes of the CMZ contain two to three times more molecular gas mass than at negative longitudes (Launhardt et al. 2002). Similar to the molecular gas, more 6.7 GHz CH_3OH masers are located towards positive Galactic longitudes, with 24 of the CH_3OH masers appearing towards positive Galactic longitudes and only 10 towards negative longitudes. In order to better visualize the distribution of the velocity and flux density of these CH_3OH masers, Figure 3 shows the location of the CH_3OH masers as colored circles, where the radii of the circles are proportional to the flux density, and the color of the circle indicates the velocity. Aside from a few bright masers near Sgr C and north of the non-thermal filament known as the Snake, all of the brightest CH_3OH masers are also located at positive Galactic longitudes.

In order to better view the velocity distribution of these CH_3OH masers, Figure 4 shows the velocities of the CH_3OH masers as a function of Galactic longitude (commonly referred to as an $l - v$ diagram). Aside from a single maser at G0.912–0.060 (ID 6 in Table 3) with a velocity of –71 km s^{-1}, all the CH_3OH masers appear to follow the same general trend of the CMZ as shown by a similar $l - v$ diagram of CII from Langer et al. (2017).

Figure 5 shows the flux density distribution (with a bin size of 0.4 Jy beam^{-1}, which is $\sim 5\sigma$). Although suffering from a small number of detections, fainter (< 1 Jy) masers appear more common. This distribution is similar to a survey done by Arecibo (Olmi et al. 2014) finding a majority of 6.7 GHz CH_3OH masers with low flux densities (< 1Jy). These low flux masers have gone undetected by previous surveys. It is likely that a population of CH_3OH masers with low flux densities may be located in the CMZ.

4.1 New 6.7 GHz CH_3OH Detections

We detected a total of 43 CH_3OH masers from 28 distinct locations. 12 of these locations already had 6.7 GHz CH_3OH masers detected towards them (see footnotes in Table 3). This leaves 16 locations with newly detected 6.7 GHz CH_3OH maser candidates that were not previously detected by the MMB survey or Caswell (2009).

There are 5 previously reported CH_3OH masers that are not detected in our survey. Figure 6 shows the locations of masers we detected as well as those detected by the MMB survey (Caswell et al. 2010). The MMB detected masers at Galactic coordinates of 358.906°+0.106°, 359.938°+0.170°, 0.376°+0.040°, 0.475°–0.010°, as well as a variety of additional positions near Sgr B2 that were not detected in our survey. There are prominent imaging artifacts near the bright CH_3OH masers[9], such as Sgr B2, and it is therefore likely that we did not include some of the CH_3OH maser detections of Caswell et al. (2010) near Sgr B2 because of confusion with these artifacts. We missed the CH_3OH maser near 0.378°+0.040°, which was only faintly detected by the MMB survey (<0.62 Jy, Caswell et al. 2010). We also did not detect the CH_3OH maser Caswell (2009) detected at 0.475°–0.010°. While it is unclear why this CH_3OH maser was not detected in our survey (their detection had a peak of 3.14 Jy near 28.8 km s^{-1}), Caswell et al. (2010) also did not list a CH_3OH maser detected at 0.475°–0.010°.

4.2 Brief Discussions of Specific 6.7 GHz CH_3OH Masers

The following sections provide brief summaries of some of the 6.7 GHz CH_3OH masers that we detected. We give a brief description of the CH_3OH maser spectra followed by comparisons to other previous detections. We compare our detections to those of Caswell (2009) and the MMB survey. We then also compared the velocities of these CH_3OH masers to that of HCN (1-0) from Jones et al. (2012). Finally, we compare the locations of these masers to 24 μm (12500 GHz) and 250 μm (1200 GHz) observations (Yusef-Zadeh et al. 2009 and Molinari et al. 2016, respectively). 24 μm emission is produced by HII regions (among other things) and 250 μm emission is produced by dust, which would also indicate the presence of molecular clouds. In the following sections, we refer to some of the ATCA detected 22 GHz H_2O masers from Rickert (2017), also see Krieger et al. (2017). The H_2O masers are collisionally pumped and are generally associated with YSOs or evolved stars.

G1.329+0.150 We identify a single CH_3OH maser at –12 km s^{-1}. Caswell et al. (2010) also detected this maser at the same location and velocity. Although this velocity does not quite match with the CMZ velocity for a Galactic longitude of 1.3 °(Langer et al. 2017), this CH_3OH maser corresponds with a HCN (1-0) cloud at this same velocity (Jones et al. 2012).

G1.282-0.084 We identify a single CH_3OH maser at –9.7 km s^{-1}. This is one of our new detections. It lies near the edge of HCN (1-0) emission at the same velocity and there is 24 μm emission present (Jones et al. 2012; Yusef-Zadeh et al. 2009). Rickert (2017) and Krieger et al. (2017) also show a new H_2O maser candidate towards this location with a velocity of –12 km s^{-1}.

Sgr D HII Region (G1.147–0.125) Sgr D is known to be composed of two parts: a northern HII region and a southern super nova remnant (SNR). While it is unclear if the two sources are physically associated with each other, both have displayed similar molecular

the visibilities as a function of time lag (and not frequency), and then Fourier transform to obtain the visibilities as a function of frequency, which can thus result in the Gibbs phenomenon appearing in the spectra (Taylor et al. 1999)

[9] Due to the sources being bright and compact and each field only being observed for short periods of time

line emission, indicating that the may be physically located near each other (Downes et al. 1980). Figure 7 shows a 90 cm continuum map of Sgr D showing the northern HII region and the southern SNR components (Law et al. 2008a). Over plotted are our detected CH_3OH (+'s) and ATCA H_2O (circles) masers (Krieger et al. 2017; Rickert 2017) along with the corresponding 6.7 GHz CH_3OH spectra. We detect a single CH_3OH maser location just southeast of (< 40″) the 90 cm emission from the edge of the northern HII regions with two spectral peaks at –19 and –15 km s^{-1}. The MMB survey detected ∼ 4 spectral peaks within –14 to –20 km s^{-1}. The –15 km s^{-1} peak coincides with the velocity of one of the ATCA detected H_2O masers, supporting that the H_2O maser would be associated with high mass star formation (Krieger et al. 2017; Rickert 2017). Figure 7 also shows that this maser is centered towards a clump of 24 μm emission, and all of the mentioned velocities coincide with HCN (1-0) emission towards this location, supporting that this CH_3OH maser is associated with a corresponding molecular cloud (Jones et al. 2012; Yusef-Zadeh et al. 2009).

Sgr D SNR (G1.008–0.237) G1.008–0.237 is located south of the 90 cm emission depicting the SNR component of Sgr D and is shown in Figure 7 (Law et al. 2008a). We detected two spectral peaks at 1.7 and 5.9 km s^{-1}. Caswell et al. (2010) detected similar peaks at ∼ 1 and 6 km s^{-1} although they resolved their 1 km s^{-1} peak into a double peak. The ∼ 1 km s^{-1} peak matches the 0.7 km s^{-1} velocity of one of the ATCA H_2O masers that was also detected from the same location (Krieger et al. 2017; Rickert 2017), supporting that it is associated with high mass star formation. There is 250 μm emission towards this location (Molinari et al. 2016).

G0.912–0.060 We identify a new CH_3OH maser at -71 km s^{-1}. This large negative velocity makes this maser unique, as it can be seen that it stands alone among the CH_3OH masers in the $l - v$ diagram of Figure 4. A comparison to similar $l - v$ diagrams of Langer et al. (2017) and Molinari et al. (2011) indicates that this maser is not associate with the CMZ. Further evidence is the lack of any HCN (1-0) emission at this velocity (Jones et al. 2012). This differing velocity is also made evident by how we detected other nearby (within 36 ″) CH_3OH masers (G0.911-0.053 and G0.909-0.061) with much different velocities of 26 and 19 km s^{-1}.

G0.9–0.0 We identify 4 additional new CH_3OH masers at locations of: G0.911–0.05, G0.909–0.06, G0.899–0.028, G0.889–0.079. Unlike G0.912–0.060, these all have velocities of: 26, 19, 42, and 12 km s^{-1}, respectively, all of which better match the velocities of the CMZ molecular gas. While at the exact locations of these masers, there does not appear to be corresponding HCN (1-0) emission at these velocities, there is corresponding emission nearby (within 50″ , 2 pc). All the masers located are near (within 3′) HCN (1-0) emission at their corresponding velocities and 250 μm emission. G0.911–0.053 is located towards a YSO candidate identified from 4.5 μm excess by Yusef-Zadeh et al. (2009). The low flux density (<0.3 Jy beam^{-1}) and narrow channel widths of G0.909–0.061, and G0.889–0.079 could indicate that these are false detections caused by channel noise and could benefit from follow up observations to confirm that they are masers.

G0.836+0.184 We detect a single CH_3OH maser at 3.6 km s^{-1}. Caswell et al. (2010) previously detected this maser, although they also detected a ∼2 km s^{-1} component that does not show up in our observations. The CH_3OH maser is co-located with 250 μm emission (Molinari et al. 2016). This position also matches the location of a YSO candidate identified by Yusef-Zadeh et al. (2009).

Sgr B2 (G0.695–0.038, G0.666–0.029, and G0.645–0.042) The Sgr B complex is the 2nd brightest radio source in the CMZ, and is broken into Sgr B1 (G0.506–0.055) and Sgr B2 (G0.667–0.036). Sgr B2 is the most prominent star forming site in the CMZ, with dozens of compact and ultra-compact HII regions (Mehringer et al. 1993). Sgr B2 is broken into three different regions: North (N), Main (M), and South (S), with Sgr B2(M) containing the most HII regions.

We identify CH_3OH masers towards three separate locations (G0.695–0.038, G0.666–0.029, and G0.645–0.042) with velocities spanning 49 to 72 km s^{-1}. Figure 8 shows the locations of our CH_3OH maser candidates superimposed on a 90 cm continuum map (Law et al. 2008a). The corresponding spectra are shown as insets. G0.666–0.029 coincides with the location of the molecular cloud Sgr B2(N) and contains two peaks at 70 and 72 km s^{-1} while G0.645–0.042 coincides with the location of the molecular cloud Sgr B2(S) and contains two peaks at 49 and 52 km s^{-1}. Green et al. (2015) and the MMB survey (Caswell et al. 2010) identified 6.7 GHz CH_3OH masers from six different locations from G0.665–0.036 to G0.677–0.025. These locations contain a variety of velocities, but they all are concentrated about 50 and 70 km s^{-1} (spanning ∼ 10 km s^{-1} about each of these two central velocities), matching with our VLA detections at G0.666–0.029, and G0.645–0.042. Houghton & Whiteoak (1995) detected a total of 11 maser locations with their ATCA observations that targeted SG B2, and all of their masers had similar velocities spanning 45 to 75 km s^{-1}. Many of the additional CH_3OH masers detected by Caswell et al. (2010) and Houghton & Whiteoak (1995) masers have similar spectra with overlapping velocity features. Such overlapping velocities would have been construed as possible artifacts in our detection method and removed from our final list of masers, which is why our maser catalog does not include as many maser locations.

Our detected CH_3OH maser at G0.695–0.038 has a single velocity at 68 km s^{-1}. Green et al. (2015), Houghton & Whiteoak (1995), and Caswell (2009) also detected a 6.7 GHz CH_3OH maser at this location, with a variety of velocities spanning 10 km s^{-1} centered at 69 km s^{-1}. This matches with some of the additional features in our spectra for G0.695–0.038 (Figure 8) that were not included in the detections, likely either because Gaussians could not be fitted to them or because of the velocity overlap with the features at G0.66–0.029. Also superimposed on Figure 8 are the locations of the ATCA H_2O masers (Krieger et al. 2017; Rickert 2017). It can be seen that G0.666–0.029 coincides with a H_2O maser (with a 71 km s^{-1} velocity, matching that of the CH_3OH maser), while the other two CH_3OH maser are offset from locations of H_2O masers.

G0.530–0.198 This is one of our newly detected CH_3OH masers. We detect a single 49 km s^{-1} maser towards this location. There is 24 μm emission less than 36″ (1.5 pc) away (Yusef-Zadeh et al. 2009). The 49 km s^{-1} velocity matches with the peak velocity of HCN (1-0) emission towards this same location, supporting that this maser is associated with the molecular cloud (Jones et al. 2012).

G0.49+0.188 We detected CH_3OH masers towards two locations (G0.497+0.188 and G0.496+0.188) with spectra near –7 and 0 km s^{-1}. The MMB survey identified a single location with a variety of spectral peaks spanning –12 to 2 km s^{-1}, although their velocities are all located primarily near –9 and –1 km s^{-1}. We are able to resolve these two clumps of spectral lines into two distinct locations located less than 4″ apart, which falls within the resolution of Caswell et al. (2010). G0.49+0.188 coincides with both 24 μm and 250 μm emission (Yusef-Zadeh et al. 2009; Molinari et al. 2016).

G0.315–0.201 We identify a maser at 18 km s^{-1}. The MMB survey detected three 6.7 GHz CH_3OH masers towards this location with velocities near 15, 18 and 20 km s^{-1}. While we only identify the 18 km s^{-1} maser, there are two low level peaks that occur near

15 km s^{-1} and 20 km s^{-1} in our spectra (Figure 9). These were not registered as detections though, likely due to the low level. The 18 km s^{-1} maser velocity matches with the peak velocity of HCN (1-0) towards this location (Jones et al. 2012). Figure 9 shows that this maser coincides with 24 μm and 250 μm emission (Yusef-Zadeh et al. 2009; Molinari et al. 2016).

G0.212–0.001 We identify a single CH_3OH maser at 49 km s^{-1}. The MMB survey identified four 4 spectral peaks towards this same location with velocities spanning 41 to 50 km s^{-1}. Additional spectral peaks are detected near 42 and 48 km s^{-1}, however these peaks are only 1-2 channels wide and can not be fitted by Gaussians, and thus are not included as detections. There are also multiple nearby (within 15″) H_2O masers (Krieger et al. 2017; Rickert 2017). One H_2O maser, contains a spectral peak at 48 km s^{-1}, matching that of our detected CH_3OH masers, indicating that this H_2O maser is associated with high mass star formation. There is HCN (1-0) emission towards this location with velocities spanning 10-95 km s^{-1} (Jones et al. 2012). This CH_3OH maser coincides with 24 μm emission (Yusef-Zadeh et al. 2009).

G359.703–0.218 We identify two CH_3OH masers with velocities of 19 and 23 km s^{-1}. There is also a faint peak near 25 km s^{-1} evident in our spectra. However this feature did not make it into our detections due to its narrow channel width. The MMB survey identified multiple CH_3OH masers towards this location with velocities spanning 14 to 27 km s^{-1}, although the MMB survey identified this CH_3OH maser at a slightly different location (359.615°-0.243°). It is unclear the reason for this ∼6′ difference in location. There is corresponding HCN (1-0) emission at these 14-27 km s^{-1} velocities indicating that these masers are likely associated with the molecular gas (Jones et al. 2012). This maser is located within 1.2′ (3 pc) of 24 μm emission (Yusef-Zadeh et al. 2009).

Sgr C (G359.394–0.075) Sgr C is known to contain a shell-like HII region located within a cavity of molecular gas (Liszt & Spiker 1995). We identify two CH_3OH masers towards a single location of the Sgr C HII region with velocities at –52 and –46 km s^{-1}. The MMB survey separated these two CH_3OH masers as coming from two locations separated by 7″ . These velocities match with those of 22 GHz H_2O masers that have been detected towards this location (Caswell et al. 2011; Taylor et al. 1993), and are near the -60 km s^{-1} velocity of the nearby molecular gas (Liszt & Spiker 1995).

G358.931–0.030 We identify three CH_3OH masers towards a single location with velocities at –18, –17, and –16 km s^{-1}. There are also fainter (< 0.1 Jy beam^{-1}) peaks (near –20, –19, and –15 km s^{-1}) that did not qualify as detections due to the low levels and narrow channel widths (the –15 km s^{-1} peak is a single channel wide). The MMB survey identified many CH_3OH masers from this single location with velocities spanning –22 to –14 km s^{-1}. There is faint (< 600 MJy/sr) 250 μm emission coincident with this maser location (Molinari et al. 2016).

G358.809–0.085 We identify CH_3OH masers with velocities at –51 km s^{-1} and –56 km s^{-1}towards a single location, although the peak at –56 km s^{-1} displays a double peak spectra. The MMB survey also identified multiple CH_3OH masers towards this location with velocities spanning –60 to –50 km s^{-1}, which our observations agree with except for their lower level (< 0.5 Jy) detection near –60 km s^{-1}, which does not show up in our observations. There is also faint (< 800 MJy / sr) 250 μm emission coincident with these masers (Molinari et al. 2016).

G358.721–0.126 We identify CH_3OH masers with velocities at 10 and 12 km s^{-1}towards a single location. The MMB survey also identified these CH_3OH masers with matching velocities of 10 and 12 km s^{-1}. Caswell et al. (2010) indicated that this velocity places the masers at a distance < 13.5 kpc and outside the solar circle, potentially placing these masers in the CMZ. There is also faint (< 800 MJy / sr) 250 μm emission coincident with these masers (Molinari et al. 2016).

5 CONCLUSIONS

Using the VLA, we conducted a blind survey of 6.7 GHz CH_3OH masers covering the inner ∼ 3°× 0.5° of the GC. This maser is an exclusive indicator of high mass star formation. We detect 43 CH_3OH masers towards 28 distinct locations. ∼16 of these are new detections, including a new group of masers located towards G0.9–0.0. We also detect CH_3OH masers towards Sgr B, Sgr C, Sgr D, and other molecular clouds that agree with previous 6.7 GHz CH_3OH masers detected towards these regions. A majority of the masers have velocities consistent with being in the CMZ. The spatial distribution of CH_3OH masers appears to show an asymmetry, with 24 CH_3OH masers detected at positive Galactic longitudes and only 10 towards negative longitudes. This is similar to how about two-thirds of the molecular gas in this region is located at positive Galactic longitudes. This work demonstrates the benefit of using blind interferometric surveys of masers to identify new sites of star formation towards the CMZ.

ACKNOWLEDGEMENTS

This work was partially supported by the grant AST-0807400 from the NSF, the National Radio Astronomy Observatory's summer student program and Grote Reber fellowship.

REFERENCES

Ao Y., et al., 2013, A&A, 550, A135
Bally J., Stark A. A., Wilson R. W., Henkel C., 1987, ApJS, 65, 13
Barnes A. T., Longmore S. N., Battersby C., Bally J., Kruijssen J. M. D., Henshaw J. D., Walker D. L., 2017, MNRAS, 469, 2263
Breen S. L., Ellingsen S. P., Contreras Y., Green J. A., Caswell J. L., Stevens J. B., Dawson J. R., Voronkov M. A., 2013, MNRAS, 435, 524
Caswell J. L., 1996, MNRAS, 279, 79
Caswell J. L., 2009, PASJ, 26, 454
Caswell J. L., et al., 2010, MNRAS, 404, 1029
Caswell J. L., Breen S. L., Ellingsen S. P., 2011, MNRAS, 410, 1283
Chambers E. T., Jackson J. M., Rathborne J. M., Simon R., 2009, ApJS, 181, 360
Chambers E. T., Yusef-Zadeh F., Ott J., 2014, A&A, 563, A68
Cotton W. D., Yusef-Zadeh F., 2016, ApJS, 227, 10
Dahmen G., Huttemeister S., Wilson T. L., Mauersberger R., 1998, A&A, 331, 959
Downes D., Wilson T. L., Bieging J., Wink J., 1980, A&AS, 40, 379
Forster J. R., Caswell J. L., 1999, A&AS, 137, 43
Green J. A., et al., 2009, MNRAS, 392, 783
Green J. A., Caswell J. L., McClure-Griffiths N. M., 2015, MNRAS, 451, 74
Harju J., Lehtinen K., Booth R. S., Zinchenko I., 1998, A&AS, 132, 211
Houghton S., Whiteoak J. B., 1995, MNRAS, 273, 1033
Jones P. A., et al., 2012, MNRAS, 419, 2961
Jones P. A., Burton M. G., Cunningham M. R., Tothill N. F. H., Walsh A. J., 2013, MNRAS, 433, 221
Krieger N., et al., 2017, ApJ, 850, 77
Langer W. D., Velusamy T., Morris M. R., Goldsmith P. F., Pineda J. L., 2017, A&A, 599, A136

Launhardt R., Zylka R., Mezger P. G., 2002, A&A, 384, 112
Law C. J., Yusef-Zadeh F., Cotton W. D., Maddalena R. J., 2008a, ApJS, 177, 255
Law C. J., Yusef-Zadeh F., Cotton W. D., 2008b, ApJS, 177, 515
Lis D. C., Menten K. M., 1998, ApJ, 507, 794
Liszt H. S., Spiker R. W., 1995, ApJS, 98, 259
Longmore S. N., et al., 2013, MNRAS, 429, 987
Martín-Pintado J., de Vicente P., Fuente A., Planesas P., 1997, ApJ, 482, L45
Martin C. L., Walsh W. M., Xiao K., Lane A. P., Walker C. K., Stark A. A., 2004, ApJS, 150, 239
McMullin J. P., Waters B., Schiebel D., Young W., Golap K., 2007, in Shaw R. A., Hill F., Bell D. J., eds, Astronomical Society of the Pacific Conference Series Vol. 376, Astronomical Data Analysis Software and Systems XVI. p. 127
Mehringer D. M., Palmer P., Goss W. M., Yusef-Zadeh F., 1993, ApJ, 412, 684
Menten K., 1991, in Haschick A. D., Ho P. T. P., eds, Astronomical Society of the Pacific Conference Series Vol. 16, Atoms, Ions and Molecules: New Results in Spectral Line Astrophysics. p. 119
Minier V., Ellingsen S. P., Norris R. P., Booth R. S., 2003, A&A, 403, 1095
Molinari S., et al., 2011, ApJ, 735, L33
Molinari S., et al., 2016, A&A, 591, A149
Morris M., Serabyn E., 1996, ARA&A, 34, 645
Oka T., Geballe T. R., Goto M., Usuda T., McCall B. J., 2005, ApJ, 632, 882
Olmi L., Araya E. D., Hofner P., Molinari S., Morales Ortiz J., Moscadelli L., Pestalozzi M., 2014, A&A, 566, A18
Rickert M., 2017, PhD thesis, Northwestern University
Sjouwerman L. O., van Langevelde H. J., Winnberg A., Habing H. J., 1998, A&AS, 128, 35
Sjouwerman L. O., Lindqvist M., van Langevelde H. J., Diamond P. J., 2002, A&A, 391, 967
Taylor G. B., Morris M., Schulman E., 1993, AJ, 106, 1978
Taylor G. B., Carilli C. L., Perley R. A., eds, 1999, Synthesis Imaging in Radio Astronomy II Astronomical Society of the Pacific Conference Series Vol. 180
Walsh A. J., et al., 2011, MNRAS, 416, 1764
Walsh A. J., Purcell C. R., Longmore S. N., Breen S. L., Green J. A., Harvey-Smith L., Jordan C. H., Macpherson C., 2014, MNRAS, 442, 2240
Xu Y., Newberg H. J., Carlin J. L., Liu C., Deng L., Li J., Schönrich R., Yanny B., 2015, ApJ, 801, 105
Yusef-Zadeh F., et al., 2009, ApJ, 702, 178
van Dishoeck E. F., Blake G. A., 1998, ARA&A, 36, 317
van Moorsel G., 2013, Technical report, Extended EVLA band coverage - C-band. NRAO

Table 1. VLA CH_3OH Survey Observation

VLA Configuration	A
Observing Date	2015 July 09
Angular Resolution	$0.86'' \times 0.29''$ (P.A. 13°)
Primary Beam FWHM	$6.75'$
Spectral Resolution	0.4 km s^{-1} (8.06 kHz)
Velocity Coverage	± 390 km s^{-1}
Average RMS	0.08 Jy $beam^{-1}$ per channel
Total Observing Time	3 hours

Table 2. Comparison of untargeted CMZ 6.7 GHz CH_3OH Maser Surveys

	Rickert2018	MMB [a]	Caswell96
Resolution[b]	$0.86''$	$0.4''$ /$24''$	$2'' \times 4''$
Channel Width (km s^{-1})	0.4	0.11/0.4	0.18
Sensitivity	0.08 Jy $beam^{-1}$	0.07 Jy/0.17 Jy	0.16 Jy

[10]

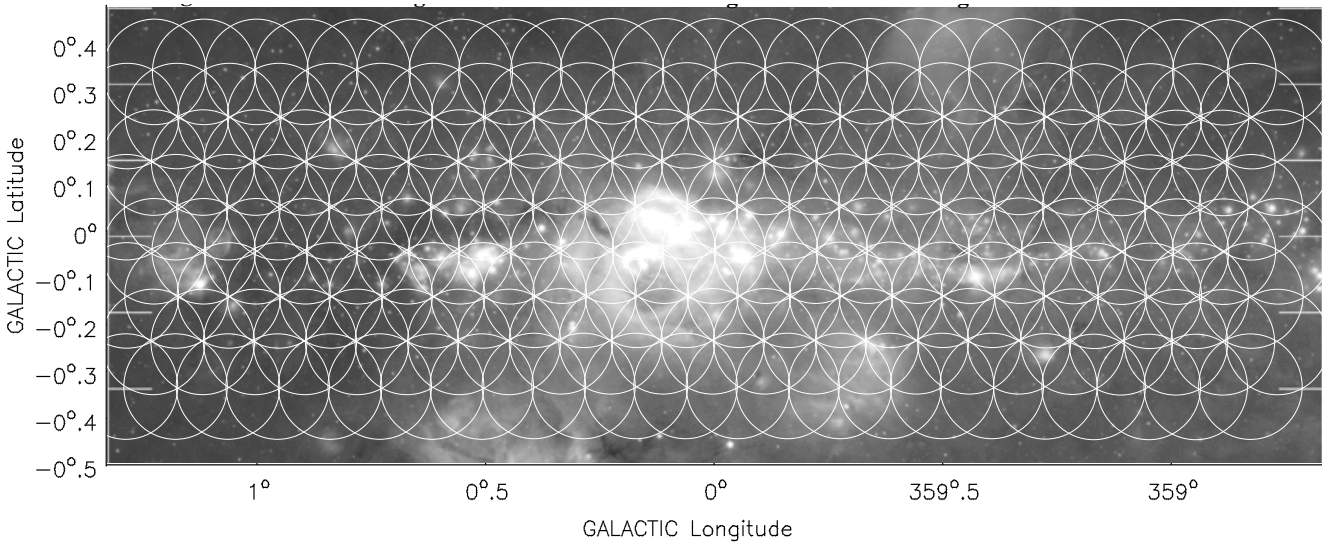


Figure 1. The observed CH_3OH fields are plotted on a 24 μm map. Each circle is roughly 6' wide, which corresponds to the primary beam at 6 GHz. At the top are labeled some prominent sources at their corresponding longitudes.

Table 3. CH_3OH Maser Spectra Gaussian Fits

ID	Source (l, b °)	RA. $h\ m\ s$	Dec. ° ′ ″	Peak Flux Density[k] (Jy beam^{-1})	RMS	V_{LSR} (km s^{-1})	FWHM (km s^{-1})	Integrated Flux (Jy s km^{-1} beam^{-1})	Peak Brightness Temperature ($\times 10^3$ K)	Associated Sources
		(J2000.0)								
0	1.329 +0.150	17 48 10.301	−27 43 20.877	0.72 ± 0.14	0.04	−12.0 ±< 0.1	0.4 ± 0.1	0.34 ± 0.10	32.4 ± 1.8	[b]
1	1.282 −0.084	17 48 58.080	−27 52 58.600	0.36 ± 0.02	0.01	−9.7 ±< 0.1	0.6 ±< 0.1	0.22 ± 0.02	16.2 ± 0.5	[j] *
2	1.147 −0.125	17 48 48.549	−28 01 11.102	0.24 ± 0.06	0.03	−19.7 ± 0.3	2.6 ± 0.8	0.50 ± 0.19	10.8 ± 1.4	Sgr D HII [a] [b] [j]
3	”	”	”	15.0 ± 1.3	0.09	−15.1 ±< 0.1	0.4 ± 0.1	6.03 ± 0.67	675.4 ± 4.1	[j]
4	1.008 −0.237	17 48 55.287	−28 11 48.192	8.05 ± 0.19	0.14	1.7 ±< 0.1	0.5 ±< 0.1	4.05 ± 0.15	362.4 ± 6.3	Sgr D SNR [a] [b] [j]
5	”	”	”	1.10 ± 0.06	0.06	5.9 ±< 0.1	0.7 ±< 0.1	0.84 ± 0.07	49.5 ± 2.7	[j]
6	0.912 −0.060	17 48 00.435	−28 11 16.945	0.11 ± 0.02	0.02	−71.3 ± 0.1	0.6 ± 0.1	0.07 ± 0.02	5.0 ± 0.9	*
7	0.911 −0.053	17 47 58.728	−28 11 04.789	0.12 ± 0.02	0.02	26.5 ± 0.1	0.4 ± 0.1	0.05 ± 0.02	5.4 ± 0.9	[c] *
8	0.909 −0.061	17 48 00.205	−28 11 27.186	0.11 ± 0.02	0.02	19.0 ± 0.1	0.4 ± 0.1	0.05 ± 0.02	5.0 ± 0.9	*
9	0.899 −0.028	17 47 51.201	−28 10 54.390	0.12 ± 0.04	0.02	42.9 ± 0.1	0.4 ± 0.2	0.05 ± 0.02	5.4 ± 0.9	*
10	0.889 −0.079	17 48 01.828	−28 13 02.861	0.12 ± 0.02	0.02	12.7 ± 0.1	0.5 ± 0.1	0.03 ± 0.03	5.4 ± 0.9	*
11	0.836 +0.184	17 46 52.826	−28 07 35.439	3.14 ± 0.05	0.07	3.6 ±< 0.1	0.4 ±< 0.1	1.24 ± 0.04	141.4 ± 3.2	[b] [c] [d]
12	0.816 −0.091	17 47 54.383	−28 17 09.354	0.08 ± 0.01	0.01	71.2 ±< 0.1	0.6 ± 0.1	0.05 ± 0.02	3.6 ± 0.5	*
13	0.695 −0.038	17 47 24.741	−28 21 43.297	11.84 ± 0.85	0.75	68.2 ± 0.1	1.7 ± 0.1	18.90 ± 3.70	533.1 ± 33.8	Sgr B2 [b] [c] [d]
14	0.666 −0.029	17 47 18.655	−28 22 54.493	24.50 ± 6.40	1.70	70.5 ±< 0.1	0.4 ± 0.1	13.1 ± 5.3	1103.1 ± 76.5	Sgr B2 [a] [b] [c] [d] [j]
15	”	”	”	5.20 ± 1.30	0.39	72.3 ±< 0.1	0.6 ± 0.2	3.5 ± 1.4	234.1 ± 17.6	[j]
16	0.645 −0.042	17 47 18.654	−28 24 24.733	36.10 ± 2.30	1.80	49.5 ±< 0.1	1.2 ± 0.1	47.8 ± 4.6	1625.4 ± 81.0	Sgr B2 [b] [c] [d]
17	”	”	”	6.82 ± 0.97	0.70	52.0 ±< 0.1	0.8 ± 0.1	11.6 ± 9.8	307.1 ± 31.5	
18	0.547 +0.261	17 45 54.060	−28 20 00.412	2.36 ± 0.15	0.03	−0.2 ± 0.1	2.2 ± 0.2	5.47 ± 0.68	106.3 ± 1.4	*
19	”	”	”	0.56 ± 0.12	0.07	−7.5 ± 0.1	0.7 ± 0.2	0.40 ± 0.19	25.2 ± 3.2	
20	0.530 −0.198	17 47 38.819	−28 35 07.443	0.21 ± 0.02	0.02	49.4 ± 0.1	1.6 ± 0.1	0.34 ± 0.04	9.5 ± 0.9	*
21	0.497 +0.188	17 46 03.989	−28 24 49.675	4.03 ± 0.64	0.16	−10.1 ± 0.4	0.6 ± 0.1	2.48 ± 0.64	181.4 ± 7.2	[b] [c]
22	0.496 +0.188	17 46 04.000	−28 24 51.899	76.10 ± 6.60	0.70	0.9 ±< 0.1	0.5 ± 0.1	39.60 ± 5.40	3426.4 ± 31.5	
23	”	”	”	2.77 ± 0.41	0.09	−7.4 ± 0.1	1.2 ± 0.2	3.46 ± 0.80	124.7 ± 4.1	
24	0.315 −0.201	17 47 09.114	−28 46 16.009	14.60 ± 1.10	0.59	18.3 ±< 0.1	0.6 ± 0.1	8.7 ± 1.1	657.4 ± 26.6	[a] [b] [c] [d]
25	0.212 −0.001	17 46 07.678	−28 45 20.390	1.056 ± 0.08	0.06	49.3 ±< 0.1	1.05 ± 0.1	1.19 ± 0.14	7.7 ± 0.5	[b] [j]
26	359.820 −0.225	17 46 04.183	−29 12 25.540	0.17 ± 0.02	0.01	19.6 ±< 0.1	0.5 ± 0.1	0.09 ± 0.021	10.4 ± 1.4	*
27	359.802 +0.188	17 44 24.806	−29 00 22.806	0.23 ± 0.03	0.03	17.5 ± 0.1	0.5 ± 0.1	0.11 ± 0.02	339.0 ± 10.8	*
28	359.703 −0.218	17 45 45.811	−29 18 10.446	7.53 ± 0.40	0.24	19.5 ±< 0.1	0.5 ±< 0.1	3.87 ± 0.33	30.2 ± 3.2	
29	”	”	”	0.67 ± 0.19	0.07	23.6 ± 0.4	2.9 ± 1.0	2.08 ± 0.94	101.8 ± 7.2	
30	359.394 −0.075	17 44 27.909	−29 29 31.299	0.68 ± 0.04	0.09	−52.2 ±< 0.1	1.0 ±< 0.1	0.70 ± 0.06	503.4 ± 30.6	Sgr C
31	”	”	”	11.18 ± 0.05	0.68	−46.7 ±< 0.1	0.5 ± 0.10	5.78 ± 0.04	594.3 ± 19.8	
32	359.138 +0.032	17 43 25.672	−29 39 17.144	13.20 ± 1.00	0.44	−3.8 ±< 0.1	0.8 ±< 0.1	10.62 ± 0.60	41.4 ± 2.7	[a] [b] [c] [h]
33	358.973 +0.088	17 42 48.433	−29 45 55.095	0.27 ± 0.04	0.05	−16.0 ±< 0.1	0.6 ± 0.1	0.18 ± 0.04	78.3 ± 2.3	
34	358.931 −0.030	17 43 10.031	−29 51 45.663	1.74 ± 0.22	0.05	−18.7 ±< 0.1	0.5 ± 0.1	1.2 ± 1.9	53.1 ± 1.8	[b]
35	”	”	”	1.18 ± 0.14	0.04	−17.3 ±< 0.1	0.7 ± 0.1	1.1 ± 1.4	139.6 ± 4.1	
36	”	”	”	3.10 ± 0.15	0.09	−16.0 ±< 0.1	0.5 ±< 0.1	1.52 ± 0.50	83.3 ± 2.7	
37	358.809 −0.085	17 43 05.408	−29 59 45.583	1.85 ± 0.21	0.06	−56.8 ± 0.1	1.9 ± 0.2	3.78 ± 0.25	9.0 ± 0.9	[b]
38	”	”	”	0.20 ± 0.32	0.02	−51.9 ± 0.6	0.8 ± 1.5	0.18 ± 0.43	27.0 ± 1.8	
39	358.721 −0.126	17 43 02.312	−30 05 29.942	0.60 ± 0.02	0.04	10.8 ±< 0.1	1.0 ±< 0.1	0.62 ± 0.04	15.3 ± 0.9	[b]
40	”	”	”	0.34 ± 0.02	0.02	12.3 ±< 0.1	1.3 ± 0.1	0.47 ± 0.06	12.6 ± 1.4	
41	358.550 +0.384	17 40 37.160	−29 58 03.303	0.28 ± 0.04	0.03	−2.4 ± 0.1	0.4 ± 0.1	0.12 ± 0.03	12.2 ± 1.4	*
42	358.539 +0.330	17 40 48.193	−30 00 20.446	0.27 ± 0.06	0.03	−36.0 ± 0.4	0.1 ±< 0.1	0.01 ± 0.03	1.8 ± 1.1	*

[a] H_2O masers: Walsh et al. 2014; 30″
[b] 6.7 GHz CH_3OH masers: Caswell et al. 2010; 20″
[c] 4.5μm YSO candidates: Yusef-Zadeh et al. 2009; 6″
[d] 6.7 GHz CH_3OH masers Caswell 2009; 2″
[e] 22 GHz H_2O and 1612 OH masers Sjouwerman et al. 2002; 2″
[f] 22 GHz H_2O and 1665 MHz OH masers Forster & Caswell 1999; 2″
[g] OH/IR stars: Sjouwerman et al. 1998; 2.5″
[h] SiO masers: Harju et al. 1998; 57″
[i] 36 GHz CH_3OH masers: Cotton & Yusef-Zadeh 2016; 0.86″
[j] H_2O masers: Krieger et al. 2017; 26″
[k] The Flux density, V_{LSR}, and FWHM are all from Gaussian fits, with fitting uncertainties.
* New detections

This paper has been typeset from a TEX/LATEX file prepared by the author.

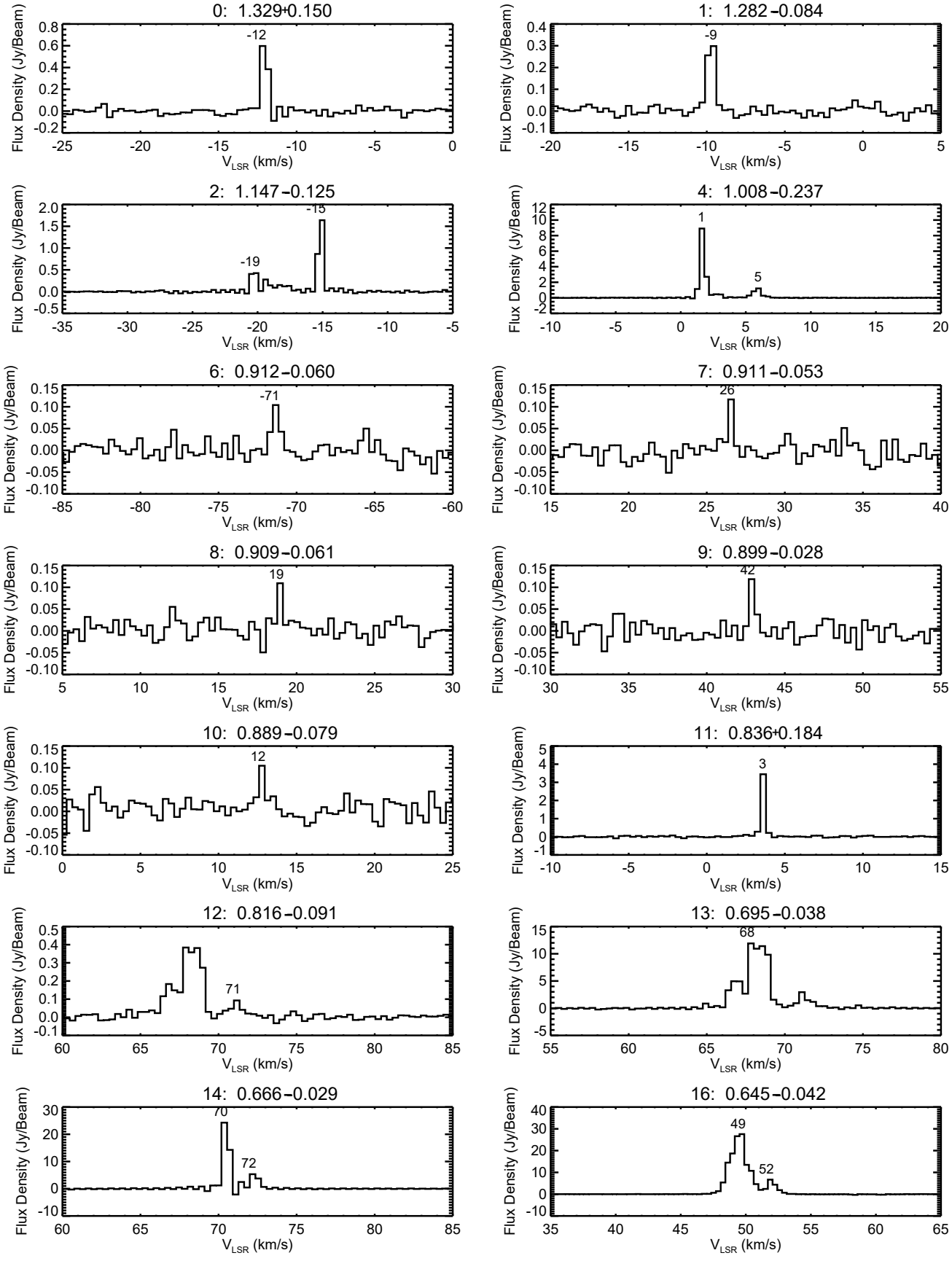


Figure 2. 27 spectra for all the 42 potential maser candidates from the blind VLA 6.7 GHz CH_3OH survey. The header gives the maser number (from Table 3 some masers are co-located; in these cases only the first maser number is listed) and the position in Galactic coordinates. The channel width is 0.4 km s^{-1}.

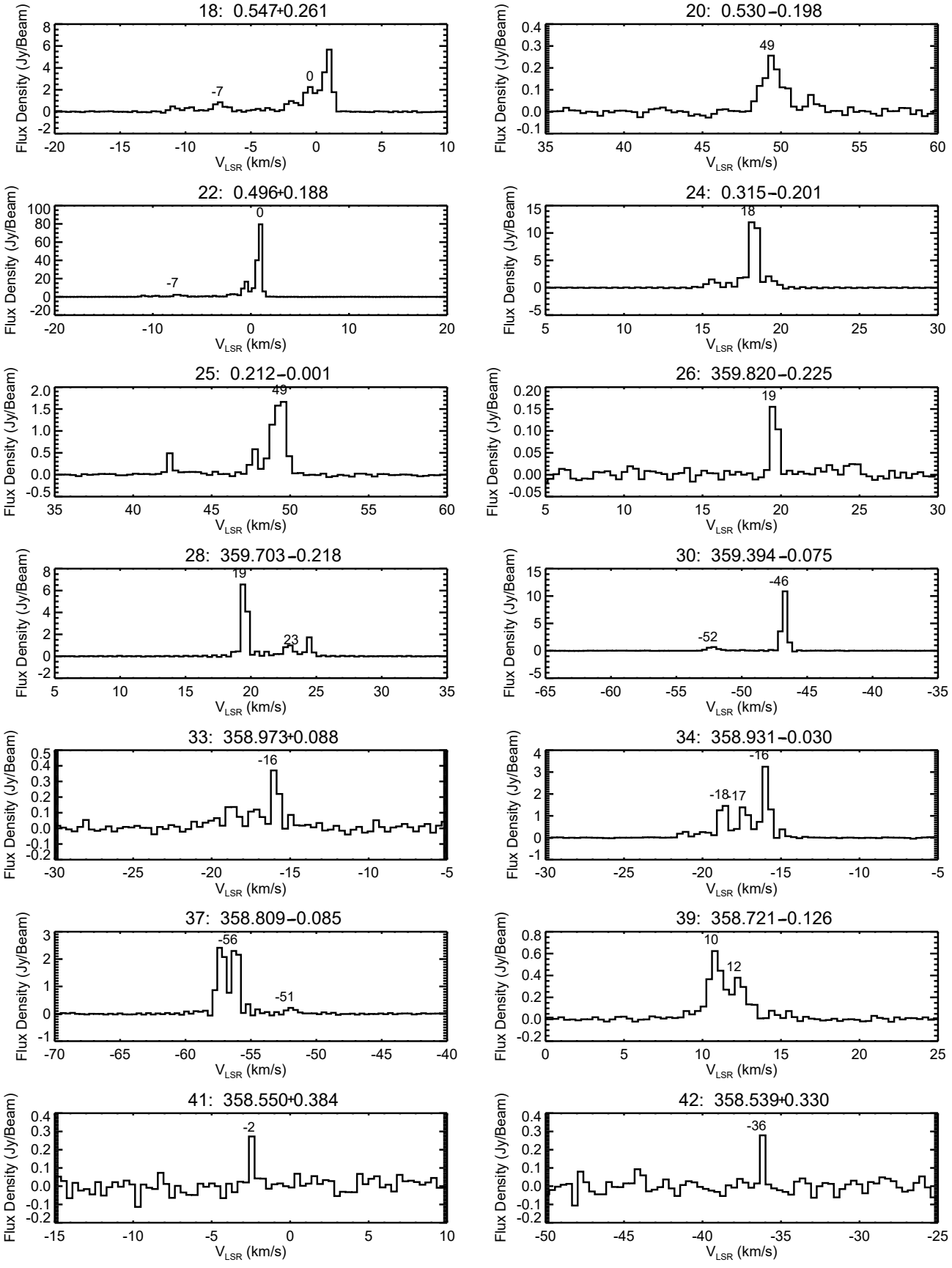


Figure 2 – *continued* Figure 2

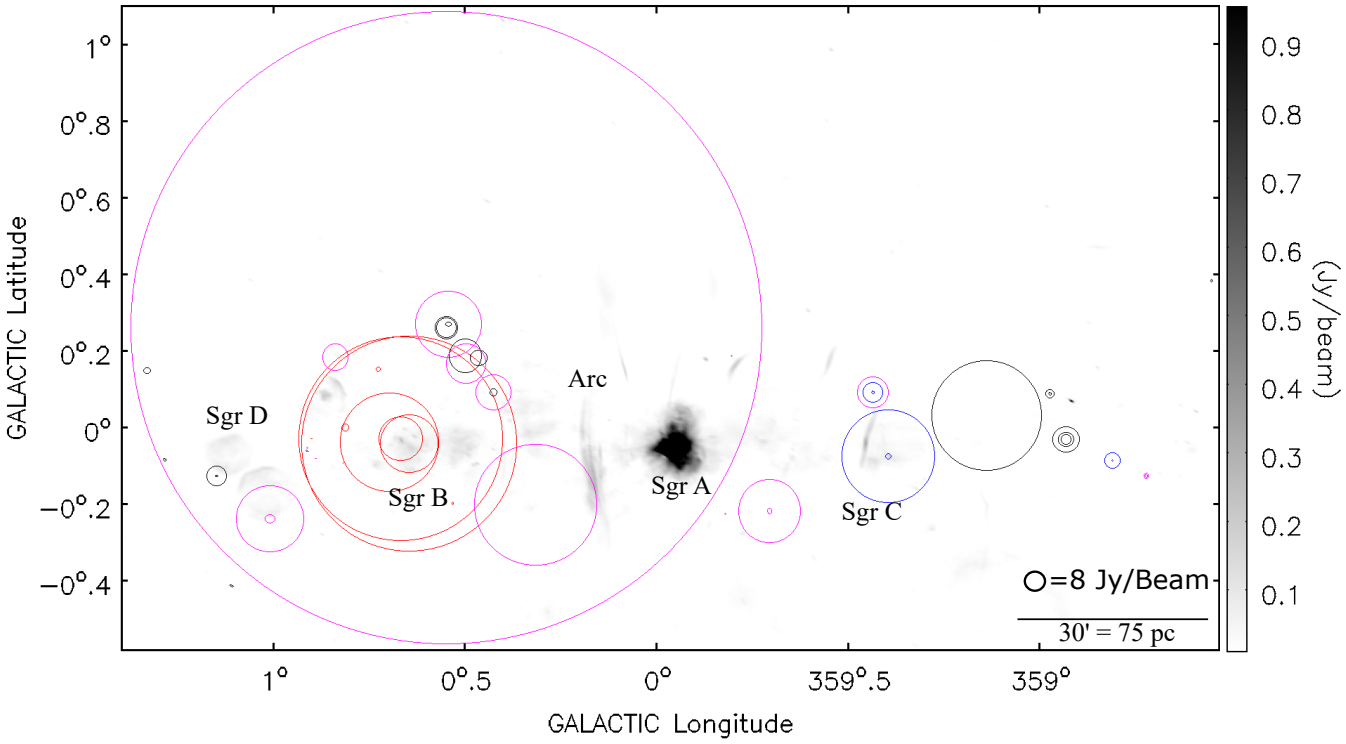


Figure 3. The detected CH_3OH masers have been plotted on a 90cm continuum map (Law et al. 2008b). The size of the circles is proportional to the maser peak flux density. The color of the circles corresponds to the maser velocity: cyan ≥100 km s^{-1}> red ≥30 km s^{-1} > magenta ≥ 0 km s^{-1} > black ≥-30 km s^{-1} > blue ≥ -100 km s^{-1} > green.

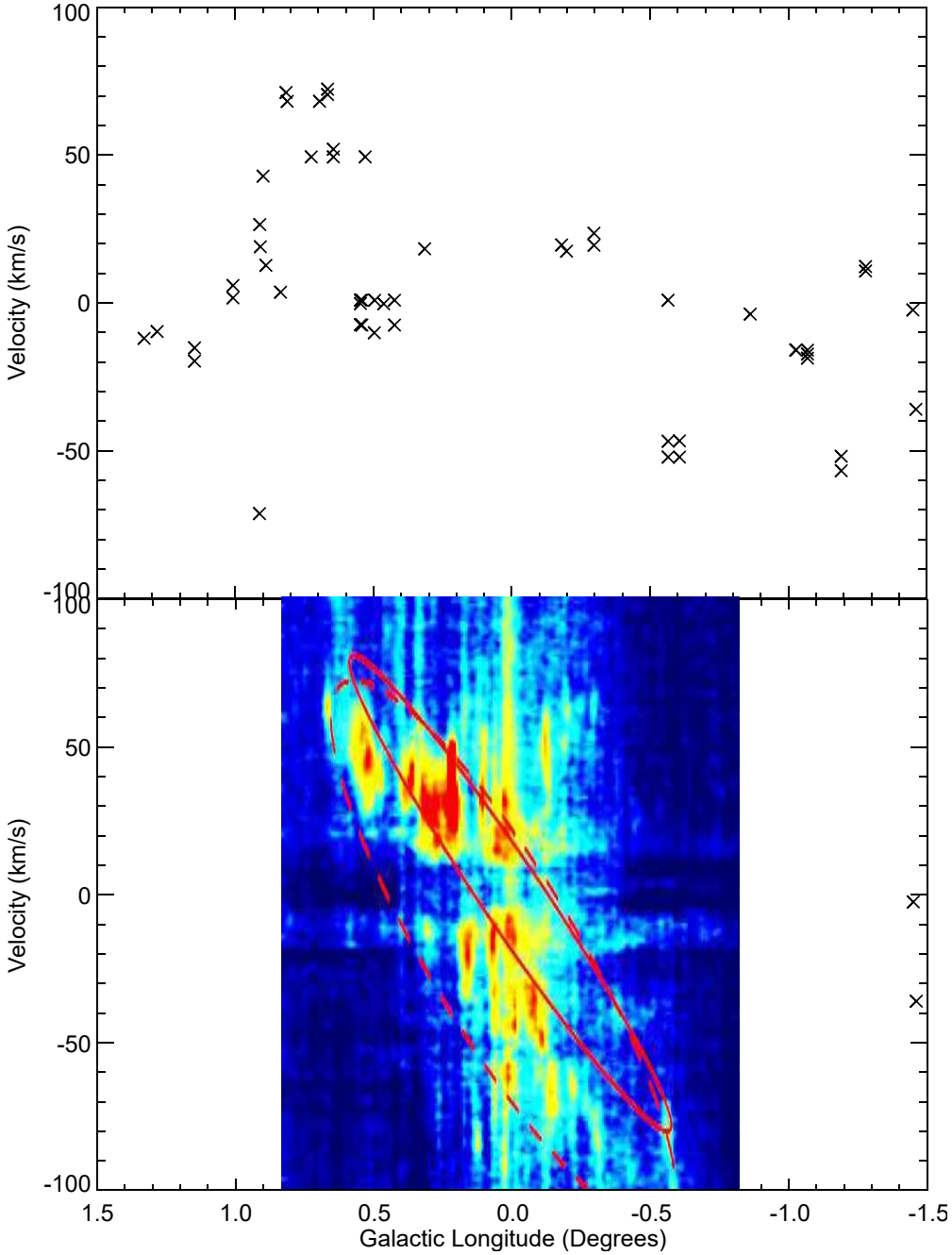


Figure 4. Top: Position - Velocity plot of our detected CH_3OH masers. **Bottom:** Position - Velocity map of CII from Langer et al. (2017) for reference (the red ellipses are two different fits to describe the kinematics of the CMZ).

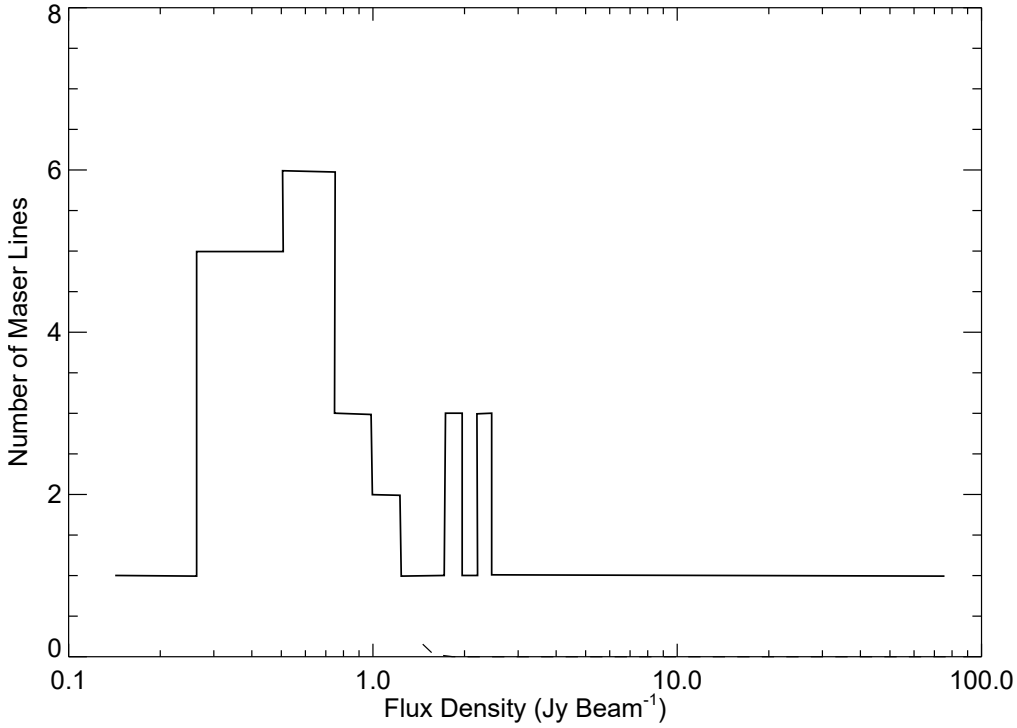


Figure 5. Histogram showing the flux density distribution of our detected CH_3OH masers from Table 3. (bin size of 0.4 Jy beam^{-1}, which is $\sim 5\sigma$).

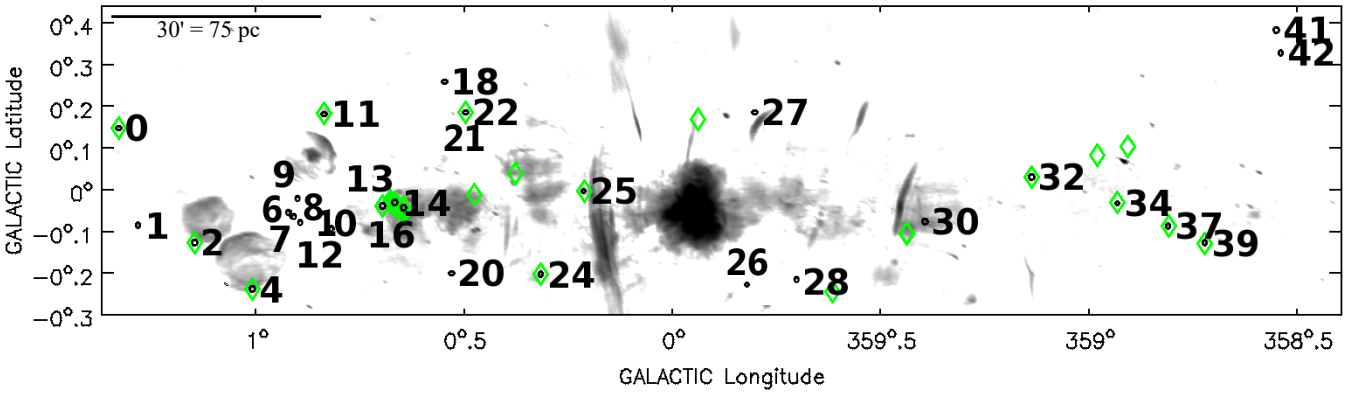


Figure 6. Our detected VLA CH_3OH masers from Table 3 (black circles) and the CH_3OH masers from the MMB survey (green diamonds) have been plotted on 90 cm continuum map (Law et al. 2008a). We detected masers towards 14 of the 22 locations that the MMB survey detected masers towards.

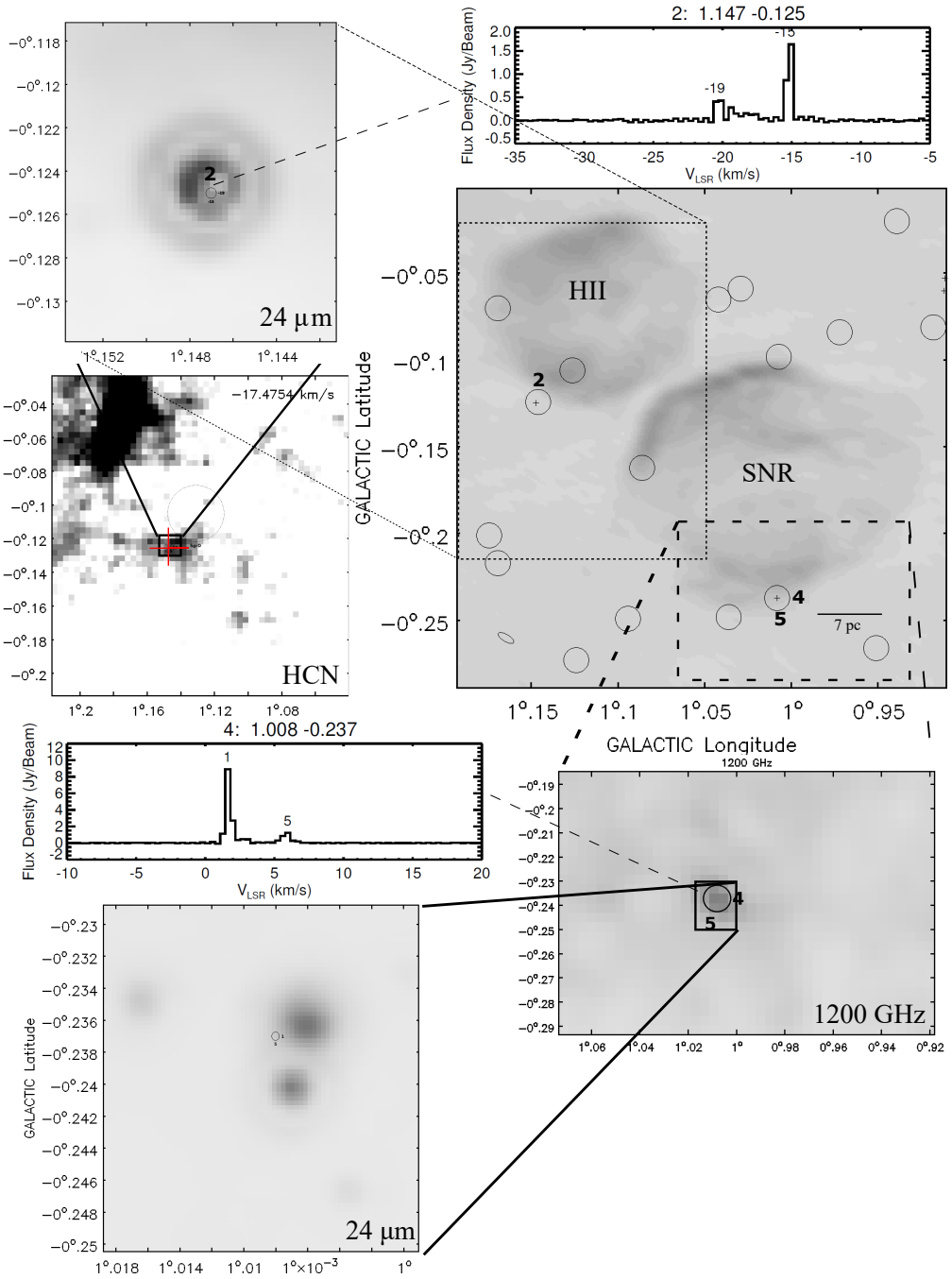


Figure 7. A 90 cm map of Sgr D (Law et al. 2008a) with the detected ATCA H_2O (circles,Krieger et al. 2017; Rickert 2017) and our VLA CH_3OH masers plotted (+'s). The northern HII region and the southern SNR are quite evident in the 90 cm map. Surrounding are the corresponding CH_3OH spectra from Figure 2. The insets correspond to: an HCN channel map (matching the corresponding CH_3OH maser velocity, 24 μm and 1200 GHz (250 μm) maps (Jones et al. 2013; Yusef-Zadeh et al. 2009; Molinari et al. 2016).

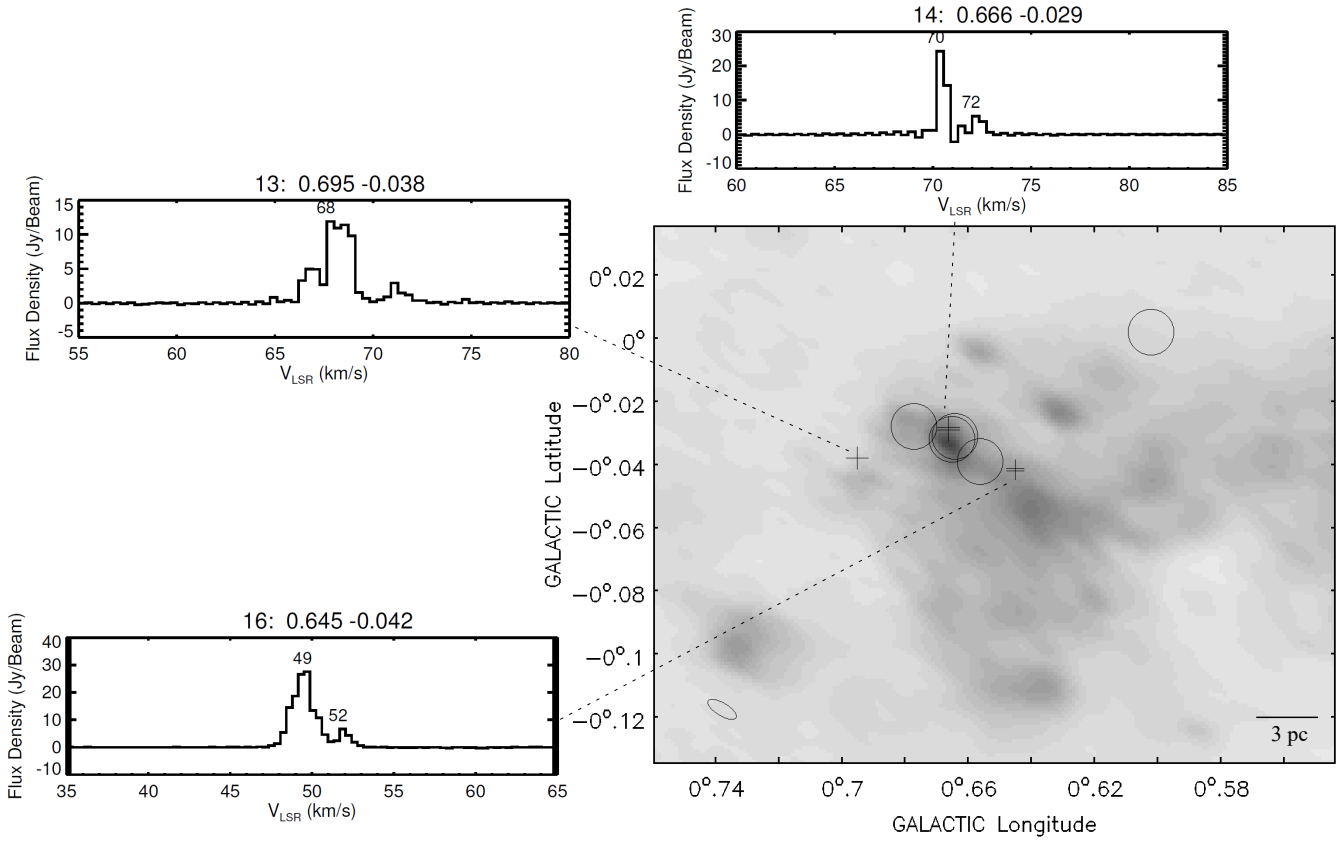


Figure 8. A 90 cm map of Sgr B2 (Law et al. 2008a) with detected ATCA H_2O (circles, Krieger et al. 2017; Rickert 2017) and our CH_3OH masers plotted (+'s). Surrounding are the corresponding CH_3OH spectra from Figure 2.

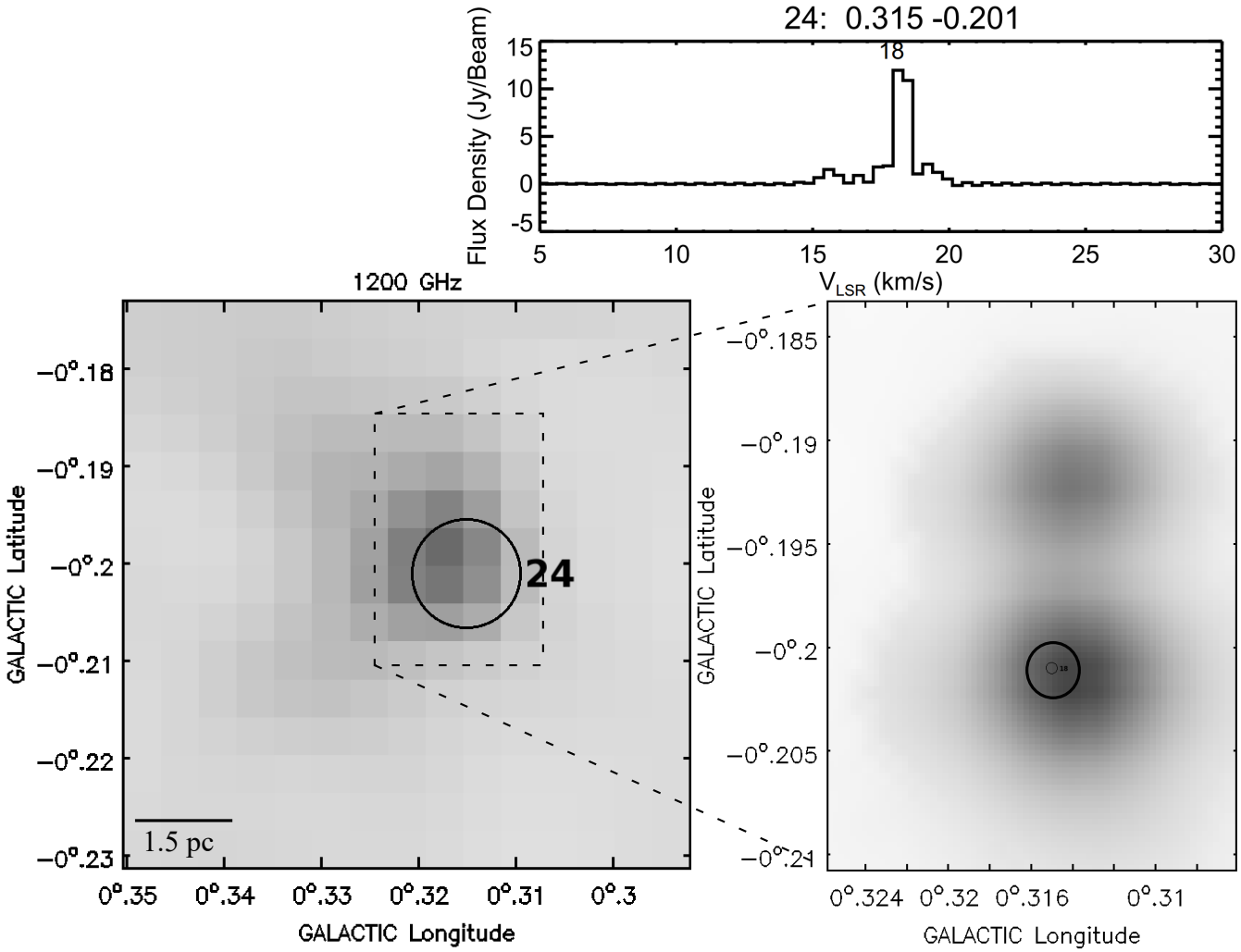


Figure 9. 250 μm and 24 μm (inset) map for G0.315–0.201 (with the corresponding CH_3OH spectrum from Figure 2 shown near the top). The position of the 18 km s^{-1} 6.7 GHz CH_3OH maser is labeled with a circle (Molinari et al. 2016; Yusef-Zadeh et al. 2009).